

## Full length article

## A defect formation mechanism induced by structural reconstruction of a well-known silicon grain boundary.



Yaoshu Xie\*, Kiyou Shibata, Teruyasu Mizoguchi

*Institute of Industrial Science, The University of Tokyo, 4-6-1, Meguro-Ku, Tokyo 135-8505, Japan*

## ARTICLE INFO

## Keywords:

Grain boundaries  
Interface phase transition  
Molecular dynamics  
Ising model  
Diamond-structured materials

## ABSTRACT

Diamond-structured grain boundaries (GBs) are important because they have notable effects on the performances of many functional devices. Previous studies have suggested that the most stable structures of some silicon GBs can be obtained by structural reconstruction from some meta-stable GBs explored at 0 K by atomic simulation. While GB reconstruction is possible to enable these meta-stable GBs to exist at elevated temperatures, reports on such behaviors are rare. This work unveiled a non-reported GB reconstruction from two degenerate ground-states of a well-known silicon GB which can be distinguished by an orientational feature of their unit structures. The reconstructing structures were verified stable by density-functional-theory (DFT) simulation. By thermodynamical and kinetical discussion, we have shown that the structural variation of this well-known GB at elevated temperatures is more likely to be dominated by this reconstruction mechanism rather than by transforming to other metastates. Such a reconstruction mechanism allows the whole GB system to be treated as an Ising model with a second-ordered phase transition. By applying harmonic transition state theory, we predicted the possible concentration of the defects induced by reconstruction at elevated temperatures and discussed their effects on the band structure of the GB by DFT simulation. An explanation was made on the cause of the difference between the phase transition behavior of this silicon GB and that of a reported copper GB. Our research made new insights into understanding the behavior of reconstructing interfaces in covalent-bonded crystalline materials.

## 1. Introduction

Since grain boundary (GB) structures play a significant role in affecting the properties of many important polycrystalline materials [1, 2], extensive studies have been done to study the structure-property relationship of GBs, where one of the main tasks is to determine their atomic structures under different physical environments. GBs in diamond-structured materials, including those in polycrystalline silicon, germanium, and diamond (carbon), have notable effects on the performances of many functional devices like solar cells and transistors [3–5], and there have been reports presenting routines to find the most stable atomic structures which are the ground states of their twist and symmetric tilt GBs at 0 K by using atomic simulation [6–8]. These previous studies have suggested that the ground state of a silicon GB can be obtained by structural reconstruction from its metastates which were attained by relaxing some initial configurations sampled from the configuration space of a coincident-site-lattice (CSL) GB, which can be distinguished by their microscopic parameters such as the relative rigid body translation (RBT) between the two adjacent crystals [9]. While

these explored meta-stable GBs with a reconstruction relationship to the ground state have been thought as unstable as they have higher GB energy at 0 K, it is questionable to ignore their presence at elevated temperatures considering the effects of entropy triggering phase transition and of kinetic energy bringing possibility for temporary existence of metastates. For CSL GBs in diamond-structured materials with well-defined structural units, a structural unit can perform reconstruction independently without requiring other units to do so simultaneously due to the stability of covalent bonds. Therefore, it is worth investigating the thermodynamical stability of a GB when its unit structures reconstruct non-simultaneously, making a structure consisting of domains like an Ising model. It is also important to reveal the probability of a single unit structure of the ground state to transform into a unit of a metastate, making a defect-like structure at elevated temperature. While there have been reports on segregation and vacancies at GBs [10,11], such defects by GB reconstruction have not been reported before. Revealing this behavior can help to discover new atomic structures and properties of GBs at elevated temperatures. Also, investigating the structural reconstruction of diamond-structured GBs can provide

\* Corresponding author.

E-mail address: [ysxie@iis.u-tokyo.ac.jp](mailto:ysxie@iis.u-tokyo.ac.jp) (Y. Xie).

new insights into studying the GB phase transitions and make comparisons with the previously reported behaviors of metallic GBs. Previous studies have reported that GBs consisting of metallic elemental materials have different GB phases [2,12], and that GB phases of face-centered cubic (fcc) and body-centered cubic (bcc) metals were explored by atomic simulation [13–15]. Furthermore, A direct observation of the coexistence of binary GB phases in copper under atomic-scale microscopy was recently achieved [16]. Despite these delightful discoveries of the phase behaviors of elemental fcc and bcc GBs, GB phase behaviors of other species of elemental materials with non-metallic bonds are still poorly understood. It is of scientific importance to extend such studies into materials with different types of chemical bonds, such as those with covalent bonds.

In this work, we show that the well-known ground state of the  $\Sigma 9(2\bar{2}\bar{1})[110]$  silicon GB splits into two degenerate states distinguished by an orientational feature reflected by the relative position of a pair of flag atoms inside the unit structure and by the relative rigid body translation (RBT) between the two adjacent crystals. Then we discussed the possibility of the coexistence of these two degenerate states at elevated temperatures considering both thermodynamical and kinetical aspects through molecular dynamics (MD) simulation. From the results, we propose a defect formation mechanism of this well-known GB imitating an Ising model by discussing the thermodynamical stability of the domain structures, the interaction between the Up and Down structural units, and the transition paths and transition rates of a single structural unit with different neighboring environments. These results provide helpful insights into understanding the structural variation of diamond-structured GBs at elevated temperatures and the differences between the phase behaviors of covalent-bonded GBs and that of metallic GBs.

## 2. Methods

### 2.1. Exploring GB states by empirical atomic potentials

GB states of the  $\Sigma 9(2\bar{2}\bar{1})[110]$  GB of silicon, germanium, and diamond (carbon) were explored following Tschopp's method [17] using LAMMPS [18] where the interaction between atoms was modeled with a modified Tersoff potential by Pun and Mishin for silicon [19], a Tersoff potential for germanium [20] and a long-range bond-order potential [21] for carbon. The atomic structures of the GBs were visualized by OVITO [22].

### 2.2. Density-functional-theory simulation

Density-Functional-Theory (DFT) simulation was conducted to compute GB energy using the projector augmented wave method and generalized gradient approximation (GGA) implemented in VASP [23, 24] with cutoff energy for the plane-wave basis set for silicon, germanium, and carbon as 390 eV, 250 eV, and 530 eV respectively. For the structural optimization, supercells were extracted from the template structures relaxed by their own empirical atomic potentials using LAMMPS except for the bridge state of the diamond (carbon), which was made by the extracted supercell of silicon and was scaled according to the lattice parameter difference between silicon and diamond (carbon) simulated by the empirical atomic potentials. The supercell includes one minimum CSL GB unit in the GB plane and a length of about 20–30 Å perpendicular to the GB plane for each of the two crystals forming the bicrystal. A vacuum region of 20 Å at one end was made for relaxing the excess volume. k-point grids included one grid along the direction perpendicular to the GB, two along the rotation axis direction, and four along the third direction. We applied a similar convention with the study on the bcc GB phases [14], where the shape and size of the simulation cell were fixed to make the GB energies of different GBs in the same material comparable. The structural relaxation was finished once the

force on every atom was less than 0.05 eV/Å. For the band structure calculation, the relaxed supercell was expanded to have two replicas along the rotation axis of the tilt GB.

### 2.3. Kinetic barrier of localized reconstruction computed by nudged-elastic-band (NEB) using MD simulation

The kinetic barrier of reconstruction used to calculate the transition rate through harmonic transition state theory (HTST) was computed by NEB using MD simulation with the code implemented in LAMMPS [25, 26]. The process includes two routines. Firstly, 14 replicas from the initial structure to the final structure were relaxed to find the minimum-energy path of transition by a force spring applied on each replica, where a parallel spring of 0.1–0.2 eV/Å<sup>2</sup> was used to generate parallel nudging force separating the replicas and an extra artificial spring of 0.1–0.2 eV/Å<sup>2</sup> was applied along the direction perpendicular to the tangent direction to prevent the paths from forming acute kinks [27]. Secondly, the replica with the highest energy climbs to the maximum point of this path to reach the saddle point. The convergence criterion is that the total generated force on every replica is lower than 0.01 eV/Å.

## 3. Results and discussion

### 3.1. Reconstruction mechanism linking two degenerate GB ground states

The supercell used to explore structures of the  $\Sigma 9(2\bar{2}\bar{1})[110]$  silicon GB is visualized in Fig. 1, followed by the atomic structures of the two explored degenerate ground states, denoted as Up and Down. While the structures identical to these two ground states are well-known and have been extensively reported [8,9,28], little attention has been paid to the physical importance of the degeneracy. It can be seen from Fig. 1 that the two states can be distinguished by an orientational feature, which can be reflected by the relative position of two flag atoms forming a dumbbell, as highlighted by the dashed circles in Fig. 1. For convenience, we state that the two flag atoms form a directional dumbbell pointing from the blue atom to the red atom, where the blue atom has lower X-coordinates than the red atom. Then, we determine the two degenerate ground states of being Up and Down according to the direction from the blue atom to the red atom projected on the (-Y) Z plane.

By MD simulation, we manually facilitated a transition process from a pure Down GB to a pure Up GB by constraining the flag atoms of all the structural units in a fixed displacing path while keeping other atoms free to be relaxed, which is visualized by Supplementary Video. This manually made transition path passes through a meta-stable bridge state denoted as Right, of which the atomic structures are shown in Fig. 1 (bottom right). Like the ground states, there also exists another degenerate bridge state which we denote as Left, shown in Fig. 1 (bottom left). The denomination of Left and Right reflects the direction pointing from the blue atom to the red atom projected to the (-Y) Z plane.

In real cases, the structural units are not likely to reconstruct simultaneously, so discussing the reconstruction for a single unit is more reasonable. It is worth mentioning that the RBTs also reflect the orientational features of the Up, Down, Left, and Right states. The Up and Down states have opposite RBTs along the Z-direction, while the Left and Right states have opposite RBTs along the Y-direction. As shown in Fig. 1, since only the bonds of the atoms in the framed blocks are rearranged during reconstruction, the whole GB core structure can be treated as a tessellation of reconstructing chains in which the atomic bonds can be reconstructed, and non-reconstructing chains, which separate the reconstructing chains. Such a character makes this GB capable of being considered a system of a series of separated one-dimensional chains of the Ising model [29].

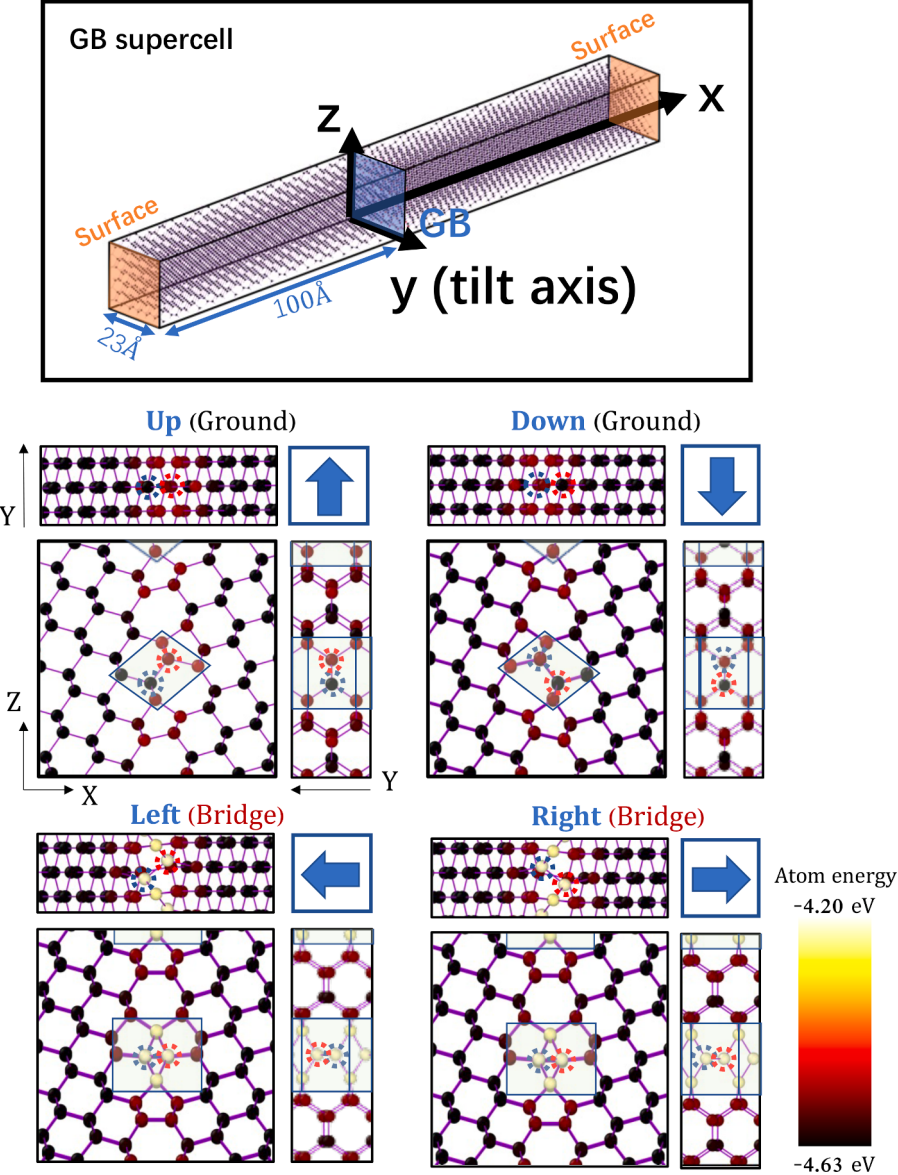


**Fig. 1.** The atomic structures of the Ground and Bridge states. The blue and red dashed circles are the flag atoms; the framed blocks are the building blocks of the reconstructing chains.

### 3.2. Atomic potential selection for MD simulation for silicon GBs and the DFT simulation results for the ground and bridge states

Our work mainly relies on MD simulations of silicon GBs, and we applied a cutoff-optimized Tersoff potential in [19], denoted as MOD/C potential, to simulate the interaction between silicon atoms. The advantages of this potential compared with others to simulate silicon systems include providing a close coefficient of thermal expansion to experimental results and being capable of reproducing results of silicon polymorphs by DFT simulation. Table 1 shows the GB energies of the ground and bridge state of silicon simulated by respectively DFT simulation, MOD/C potential, and three other famous potentials denoted as Tersoff [30], MOD [31] and SW [32] for silicon. The results show that

MOD/C potential provides closer GB energy to the DFT results than MOD and SW potentials. Tersoff potential provides closer GB energy than MOD/C for the ground state, but its error for the bridge state is larger than MOD/C. Considering the resulting GB energy, MOD/C and Tersoff seem to have similar suitability. However, because the MOD/C potential performs better in predicting other properties at elevated temperatures like the melting point, Cauchy pressure, and the coefficient of thermal expansion [19], we selected MOD/C potential for the MD simulation of silicon GBs in this work.

To investigate the universality of the results from this work in other diamond-structured materials, we also simulated the ground- and bridge-state GBs for the germanium and diamond (carbon) by DFT. The results verified their stabilities, and the calculated GB energies are

**Table 1**

GB energies of ground and bridge states of the silicon GB simulated by DFT and empirical potentials (unit: J/m<sup>2</sup>).

| Ground |       |         |       |       | Bridge |       |         |       |          |
|--------|-------|---------|-------|-------|--------|-------|---------|-------|----------|
| DFT    | MOD/C | Tersoff | MOD   | SW    | DFT    | MOD/C | Tersoff | MOD   | SW       |
| 0.190  | 0.355 | 0.134   | 0.429 | 0.451 | 0.753  | 0.908 | 0.563   | 1.103 | Unstable |

**Table 2**GB energies computed by DFT (unit: J/m<sup>2</sup>).

|           | Ground | Bridge |
|-----------|--------|--------|
| Silicon   | 0.190  | 0.753  |
| Germanium | 0.072  | 0.699  |
| Carbon    | 1.164  | 6.108  |

shown in **Table 2**. Since the DFT results have demonstrated that both ground and bridge states are reasonable structures not only for silicon but also for germanium and diamond (carbon), we believe that the reconstruction mechanism of the silicon GB discussed in this work is plausible to be further extended to germanium and diamond (carbon) GBs.

### 3.3. Thermodynamical stability of the domain structure and the interaction between neighboring Up and Down domains

To discuss the possibility of this silicon GB having domain structures like that in an Ising model, starting from a pure Up supercell containing  $Y \times Z = 12 \times 4$  replicas of units as shown in **Fig. 2** (top), we divided the two-dimensional GB structure into four square domains and constructed

four representative GB states by setting up the Up/Down orientations of the structural units in each domain as expressed by the colored arrows. We denote them as mixed supercells. Then, we calculated their GB free energies using a quasi-harmonic-approximation (QHA) method reported in [33], and compared their free energies with that of the pure Up supercell, as shown in **Fig. 2** (bottom). It can be seen from **Fig. 2** that the curves of all the four mixed supercells intersect with the pure Up curve at temperatures ranging from about 1300 K to 1450 K, which indicates phase transitions. In other words, at a temperature higher than this point, a mixed domain structure is more thermodynamically stable than a pure-Up or pure-Down ground state. Furthermore, the curves of the four mixed supercells also intersect, which means that the most stable domain structure can be temperature-dependent and thus indicating a second-order-like phase transition mechanism. This is important because almost the recently reported phase transitions of GBs in fcc and bcc elemental materials are first-ordered [13,14,16]. This disparity indicates an intrinsic difference in phase behaviors between the metallic GBs and covalent-bonded GBs, which will be discussed in 3.5.

Jian et al. [9] have suggested the importance of the metastates explored at 0 K in affecting the behavior of a GB at an elevated temperature where these states can be regarded as existing in a configurational space. Therefore, while focusing on the metastates made by

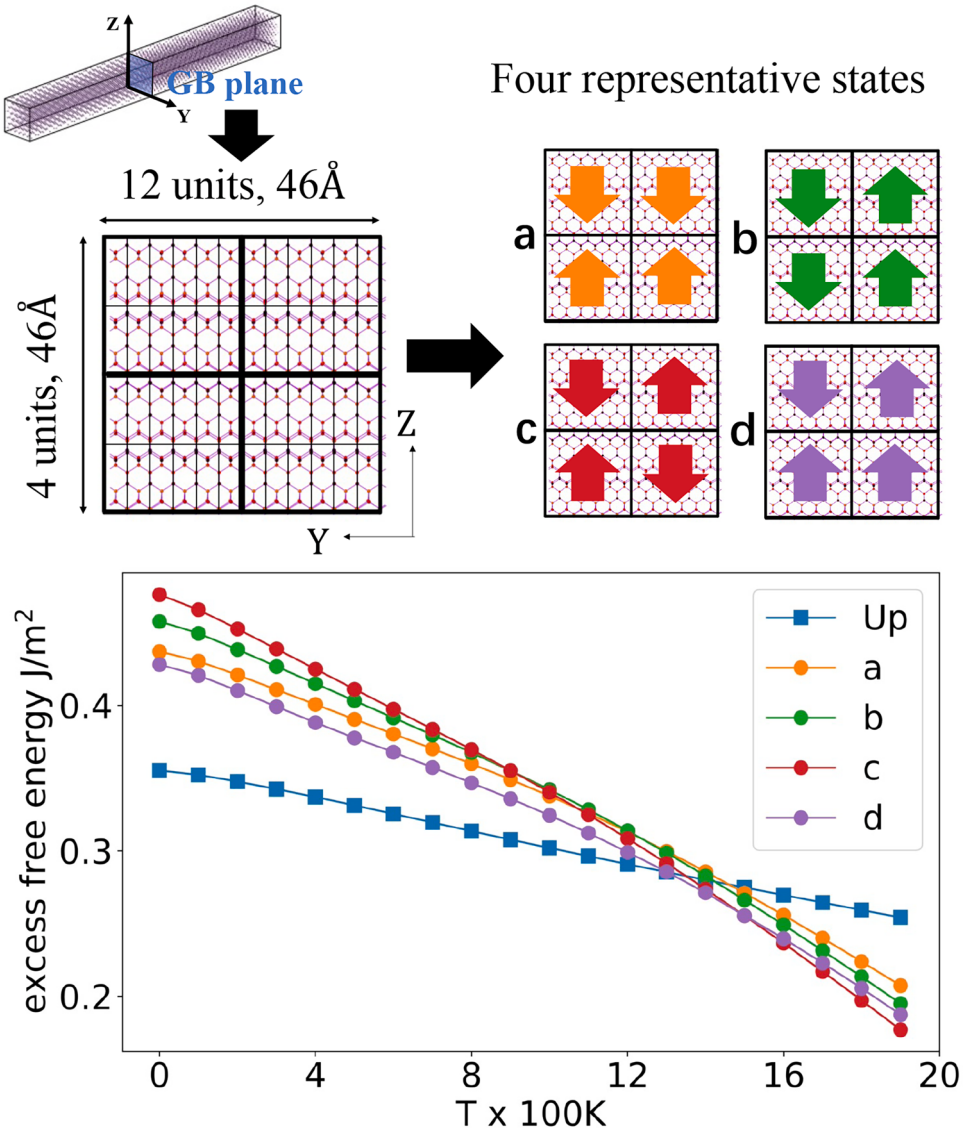


**Fig. 2.** Calculated GB excess free energy of the pure Up state and four representative reconstructed states by mixing Up and Down domains.

All the states attained by Tschopp's method

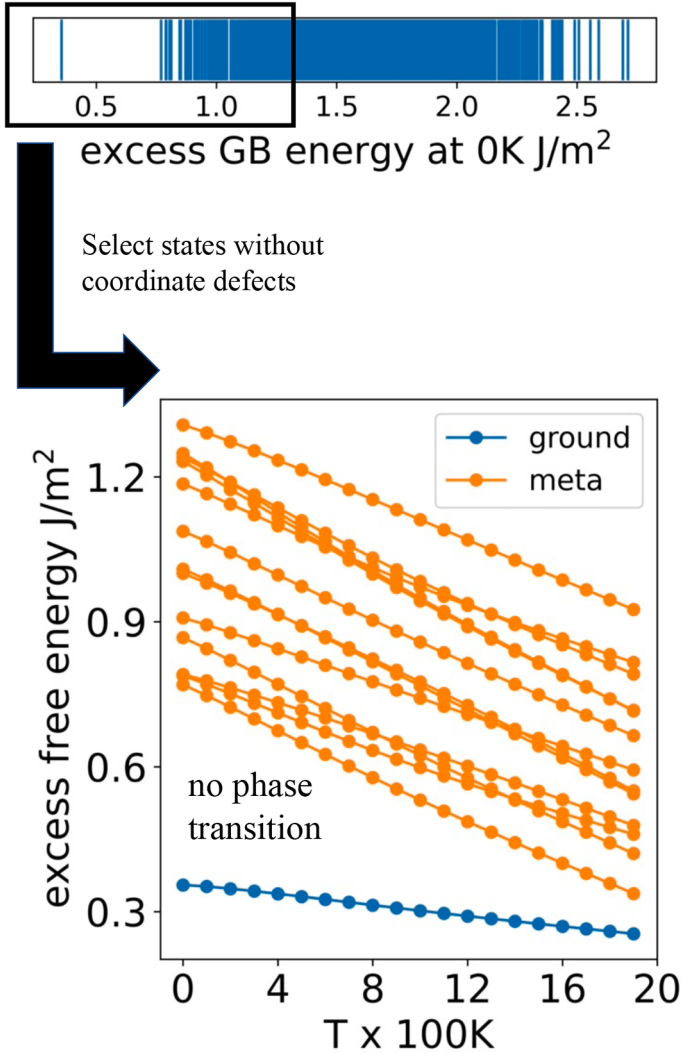


**Fig. 3.** Calculated GB free energy of the ground state and the metastates explored by Tschopp's method.

mixing Up and Down states, we also considered the possibility of phase transitions induced by other metastates which were the side products generated while we were exploring the ground and bridge states using Tschopp's method. Note that these explored GBs should have included all those reported in [9] by the 'conservative sampling' method. Fig. 3 (top) illustrates the GB energy of all the explored GB states at 0 K, from which we selected the states satisfying the condition that all the atoms have four-fold coordinates and the GB energy is lower than 1.4 J/m<sup>2</sup>, and we calculated their GB free energies at elevated temperatures by QHA, as shown in Fig. 3 (bottom). As can be seen, none of the selected metastates' curves intersect with the ground state's, which indicates that these metastates are not likely to induce phase transition at elevated temperatures. Also, according to the average entropy of these metastates, which is reflected by the curve slopes, other non-selected GBs with even higher GB energy at 0 K are either not likely to have their curves intersect with the ground state's curve because the entropy effect is not significant enough to compensate even larger internal energy difference. Fig. 3 shows that these metastates' absence of phase transition is evidently due to their much higher internal energy than the ground state.

Free energy discussion is from a thermodynamical aspect. Regarding kinetics, one can consider these metastates possible to make defects by transforming a unit structure of the ground state into a unit structure of a

metastate, which makes a temporarily existing defect-like structure. For the metastates other than the ground and bridge states made by Tschopp's method, although their structural unit has the same size as the ground-state unit, their atomic structures are incompatible with the ground-state unit. Whether two GB states are compatible depends on whether the atoms at the boundary of their structural units have the same bond arrangements. The four reconstructing states of Up, Down, Left, and Right, are compatible because they have differences in the bond arrangement of only two flag atoms inside the structural unit. When they coexist in one supercell, every atom can be allocated into one of the four well-defined structural units. On the other hand, the structural units of other metastates have different boundary-atom-bond arrangement from that of the ground-state unit. Hence when a ground-state unit is replaced by a unit of any of these metastates, such a defect can only be stabilized by introducing an extra 'interface structure' between this unit and its adjacent ground-state units. This interface structure belongs to neither the replacing metastate nor the neighboring ground states. In other words, the transition from the ground state to a non-bridge metastate goes through a complex path and requires overcoming an 'interface' energy barrier [34]. On the other hand, the transition from the ground state to a metastate with mixed Up and Down units has only two flag atoms inside each unit to be significantly displaced, thus without generating extra 'interface' structures, though they

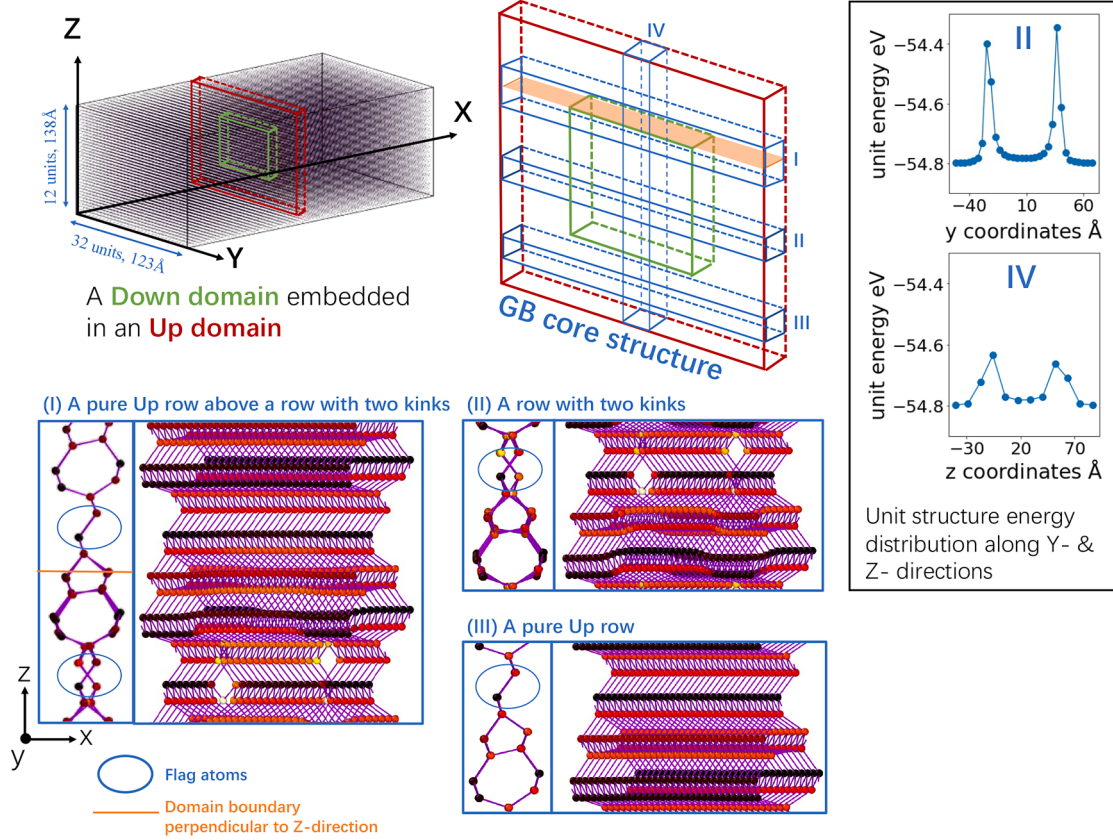


**Fig. 4.** The core structure of a GB made by embedding a Down domain in an Up domain. The scatter plots show the energy-per-unit distribution along the Y- and Z-directions of the II-row and IV-column.

do involve an extent of lattice distortion, which is analogous to the strain effects in the Ising model. In this way, from the kinetical aspect, the metastates made by mixing Up and Down units also have more significant effects on making defect-like structures at elevated temperatures because they are likely to have lower transition barriers.

The energy difference at 0 K between a GB made by mixing Up and Down units and a GB made by purely Up or purely Down units can be derived from the interaction between the oppositely oriented domains.

**Fig. 4** shows a relaxed supercell with a Down domain embedded in a larger Up domain. **Fig. 4(I)** shows the atomic structure of a pure Up row on top of a row alternating an Up and a Down segments; **Fig. 4(II)** visualizes a row crossing the embedded Down domain; and **Fig. 4 (III)** visualizes a row inside the Up domain. From **Fig. 4(II)**, a kink along the Y-direction causes notable distortion to its adjacent structural units, making a wave-like shape penetrating several unit structures along the Y-direction. According to **Fig. 4(I)**, such a distortion reflected by a penetrating wave is not notable along the Z-direction. It shows that the distortion cannot penetrate the first neighboring unit on the top of the kink. The scatter plots illustrate the per-unit-energy distribution along Y- and Z-directions. Although the penetration of the distortion along the Z-direction is not notable from **Fig. 4(I)**, both scatter plots show two peaks with tails with close lengths of about 15 Å. This indicates that the kinks along Y- & Z-directions have similar scales of strain fields. Considering the dimension of structural units along Y- & Z-directions, this strain field can penetrate several units along the Y-direction. In contrast, the first unit along the Z-direction almost terminates it.

Since the kink energy, reflected by the height of peaks, along the Y-direction is about twice the kink energy along the Z-direction, the short-range interaction along the Y-direction should be more significant than that along the Z-direction. In 3.4, we will discuss the effect of this short-range interaction on the reconstruction. Apart from the short range-interaction, opposite domains also share a long-range interaction by

the mismatch of their favorable RBTs, which makes a difference in the heights of the two plateaus in each scatter plot. Since this supercell possesses more Up states than Down states, the RBT of this supercell is closer to the RBT of a pure Up state than that of a pure Down state. Therefore, in the scatter plot, the plateau in the Down domain is higher than in the Up domain. It is worth mentioning that there is no limitation in the range of this long-range interaction because all the structural units share it in the supercell.

#### 3.4. The reconstruction rate of a structural unit estimated by HTST

In 3.3, we have shown the possibility of this well-known GB to have a second-ordered phase transition by structural reconstruction from a pure Up or pure Down GB to a mixture of them at elevated temperatures by free energy calculation. In this chapter, we apply HTST [35] to predict a single unit structure's transition rate under several distinguishable neighboring environments. Firstly, we constructed a pure Down GB supercell made by replicas of  $Y \times Z = 10 \times 6$  structural units and simulated a transition where one of the structural units goes through a transition path Down-Left-Up. Considering the symmetry, this path is equivalent to another path, Down-Right-Up. Using a multi-step NEB method through LAMMPS, we determined the minimum-energy path of this nucleation-like process. **Fig. 5(a)** illustrates that this path consists of four basin structures: Down-Left-High-Up. High is a new metastate in a shallow high-energy well, resulting from the minimum-energy path requiring the two atoms to rearrange their bonds one after the other. Note that although High is compatible with the ground state, it did not appear in the explored metastates by Tschopp's method, as it cannot form a pure and stable state of itself. After finding the minimum energy path, we confirmed that all the saddle points (SPs) obtained by the NEB simulation are well-defined by verifying that at every SP, there exists and only exists one imaginary phonon [36]. Structures of the basin

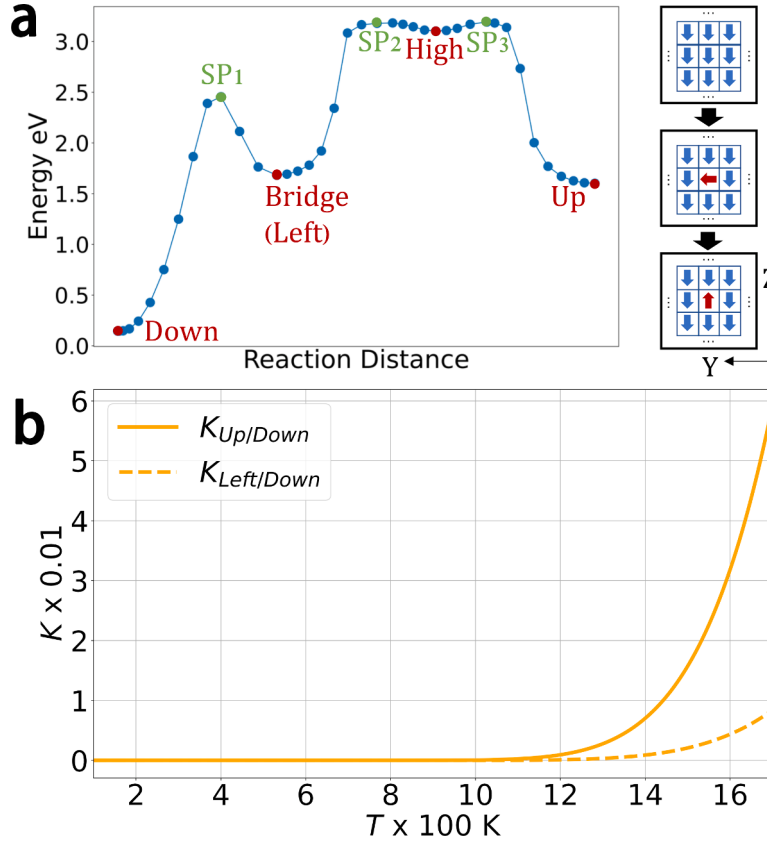


**Fig. 5.** (a) Minimum-energy path to nucleate one Up-unit in a pure Down- GB; (b)  $K_{Up/Down}$  and  $K_{Left/Down}$  as functions of temperature.

structures and SPs are visualized in Supplementary Material S1.

According to HTST, for a unit structure located at a basin  $m$  in the energy landscape, its jumping rate to the transition state which is the SP between itself and an adjacent basin is:

$$k_{m \rightarrow SP} = v_{m \rightarrow SP} \exp\left(-\frac{E_{m \rightarrow SP}}{k_B T}\right)$$

$k_{m \rightarrow SP}$  is in the unit of 1/s, which is the frequency of the current system at state  $m$  jumping to the SP.  $v_{m \rightarrow SP}$  is a pre-factor in the same unit of  $k_{m \rightarrow SP}$ , which can be determined using the Vineyards' method [36].  $E_{m \rightarrow SP}$  is the kinetic barrier in the unit of eV from the state  $m$  to the SP.  $k_B$  is the Boltzmann constant in the unit of eV/K. Here, we calculated the jumping rate from all the minimums shown in Fig. 5 to their nearby SPs at different temperatures, which are  $k_{Down \rightarrow SP_1}$ ,  $k_{Left \rightarrow SP_1}$ ,  $k_{Left \rightarrow SP_2}$ ,  $k_{High \rightarrow SP_2}$ ,  $k_{High \rightarrow SP_3}$ ,  $k_{Up \rightarrow SP_3}$ . The calculated pre-factors and kinetic barriers are listed in Table 3. With these results, we are interested in two equilibrium constants under different temperatures: the ratio  $K_{Left/Down}$  of the number of Left-states to the number of Down-states; and the ratio  $K_{Up/Down}$  of the number of Up-states to the number of Down-states. The formulas are:

$$K_{Left/Down} = \frac{k_{Down \rightarrow SP_1}}{k_{Left \rightarrow SP_1}}$$

$$K_{Up/Down} = \frac{k_{Down \rightarrow SP_1} k_{Left \rightarrow SP_2} k_{High \rightarrow SP_3}}{k_{Left \rightarrow SP_1} k_{High \rightarrow SP_2} k_{Up \rightarrow SP_3}}$$

As shown in Fig. 5(b), the calculated  $K_{Left/Down}$  and  $K_{Up/Down}$  illustrates that starting from a pure Down-GB, it requires a temperature higher than 1000 K to dynamically stabilize a composition of more than 0.1% units nucleated to become Left or Up. Also, as expected, at dynamical equilibrium, Up-defects' composition is much higher than Left- and Right-defects'.

It is plausible to regard the Up unit appearing by reconstruction as a nucleated defect because it causes a localized orientation disorder and generates an extra strain field. Now, we consider the same transition process of a structural unit next to this nucleated defect and determine whether this nucleated defect can lower the transition barrier of the neighboring unit as if it can facilitate a growth-like behavior. Since the GB is two-dimensional, the choice of the growth site can be along either Y- or Z-direction. Also, as can be seen in Fig. 6(a), because the existing Up nucleus destroyed the symmetry of its neighboring units along the Y-direction, which had been in an XZ-mirror plane before the Up-nucleus appeared, the transition paths of the neighboring units through Down-Left-Up and Down-Right-Up become non-identical. Comparably, these two paths remain identical for the neighboring units along the Z-direction because they still lie in a mirror plane. Here, we applied the same NEB method and calculated the minimum-energy paths of the Down-

**Table 3**  
Calculated  $v_{M \rightarrow SP}$  (1/s) and  $E_{M \rightarrow SP}$  (eV).

| $v_{Down \rightarrow SP_1}$ | $v_{Left \rightarrow SP_1}$ | $v_{Left \rightarrow SP_2}$ | $v_{High \rightarrow SP_2}$ | $v_{High \rightarrow SP_3}$ | $v_{Up \rightarrow SP_3}$ |
|-----------------------------|-----------------------------|-----------------------------|-----------------------------|-----------------------------|---------------------------|
| $3.11 \times 10^{15}$       | $1.03 \times 10^{13}$       | $1.19 \times 10^{13}$       | $3.29 \times 10^{12}$       | $1.74 \times 10^{12}$       | $1.53 \times 10^{12}$     |
| $E_{Down \rightarrow SP_1}$ | $E_{Left \rightarrow SP_1}$ | $E_{Left \rightarrow SP_2}$ | $E_{High \rightarrow SP_2}$ | $E_{High \rightarrow SP_3}$ | $E_{Up \rightarrow SP_3}$ |
| 2.31                        | 0.77                        | 1.50                        | 0.0810                      | 0.0900                      | 1.59                      |

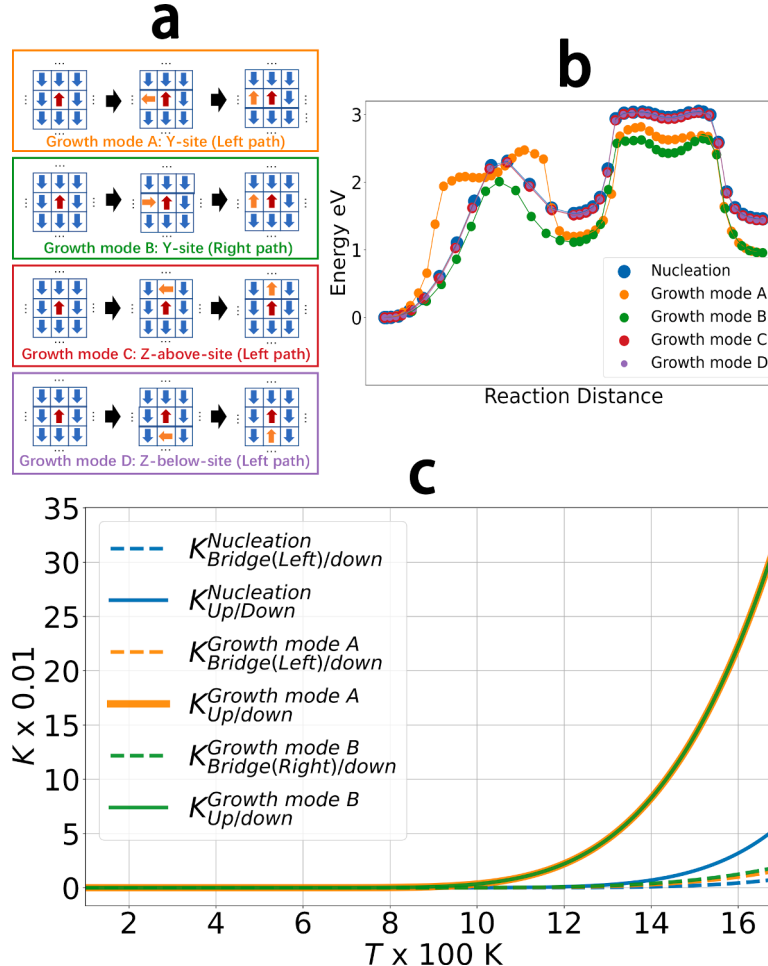


**Fig. 6.** (a) four different growth paths (b) minimum-energy-path compared with the nucleation process (c) equilibrium constants.

Left/Right-Up transitions for the unit at the left of this Up nucleus. These are identical to transitions of the Down-Right/Left-Up transitions of the unit at the right of this Up-nucleus. We also calculated the minimum-energy path of the Down-Left-Up transitions for the two units above and below the Up-nucleus. These are identical to their Down-Right-Up transitions. Fig. 6(b) shows the NEB results of all the transitions. As can be seen, the two Z-site growth paths are nearly identical to the nucleation path, verifying that the nucleus has little effect on the neighboring units along the Z-direction due to the separation of the reconstruction chains. On the other hand, the Y-site growth is significantly affected by the nucleus, which can notably lower the transition barrier and promote the equilibrium constant, as shown in Fig. 6(b) and (c). Such an anisotropy of short-range interaction verified our assumption that this GB could be regarded as a structure comprising separated one-dimensional chains of the Ising model. As mentioned above, symmetry breaking makes the growth modes by left and right paths non-identical. A significant difference is that for the unit at the left of the nucleus, the left path has one more extra high-energy state between the Down and the Left states, reflecting non-simultaneous reconstructions involving the two flag atoms. This complexity results in a higher energy barrier than the right path. However, their equilibrium constants calculated by HTST are trivially identical, only depending on the final and the initial states.

It can be predicted that the neighboring unit of this grown-up nucleus comprising two Up units, the second-neighboring unit of the firstly nucleated Up unit, can have an even higher transition rate than the first-neighboring unit because the short-range interaction can penetrate several unit structures along Y-direction. Also, as more Up units appear,

the long-range interaction by RBT can have notable effects on reconstruction. However, such a domain formation process to have a nucleus to grow up is a complex multi-step process, and investigating its kinetics is a complicated task beyond our work. Although we keep skeptical about the capability of domain formation concerning its kinetics, for this new defect formation mechanism by reconstruction of this well-known silicon GB, we have made these conclusions:

- 1) A notable number of defects by transforming a single unit structure to a bridge (Left or Right) or an oppositely oriented ground state can exist at high temperatures.
- 2) An already reverted neighboring unit can lower the kinetic barrier to revert a single unit.
- 3) The GB free energy results in 3.3 provide evidence for the thermodynamical stability of mixed domain structures at high temperatures, indicating a second-ordered phase transition.

### 3.5. Discussion on the principles of the disparity of silicon and copper GB phase transitions

Meiners et al. [16] recently reported a non-diffusive phase transition of a copper GB which was observed through an atomic-scaled microscopy image. In our work, we proposed a phase transition mechanism of a silicon GB by reconstruction between Up and Down states which is also non-diffusive. In 3.3, we have shown that this silicon GB has a second-ordered phase transition, while that copper GB's phase transition was reported to be first-ordered in [16]. Here we discuss why that copper GB's phase transition is first-ordered and the intrinsic differences

between these two materials causing disparate GB phase behaviors. For convenience, the discussion is under the constant-volume assumption, primarily applied in previous studies on GB phases.

For the copper GB reported in [16], the phase transition is induced by the difference in the Helmholtz free energies of its two physically non-identical GB states with distinctive unit structures [16,33]. Because both states have well-defined unit structures, their free energy curves are uniquely determined, thus ending up with a unique phase transition temperature. Though the transition process is non-diffusive that a bijection can be established between their unit atoms, it involves significant relative displacement of almost the atoms to transform from one unit structure to the other, which is a much more complex path than the reconstruction between the Up and Down units of the silicon GB where only two flag atoms are significantly displaced. In this way, when the two distinctive copper GB states coexist adjacently, the huge mismatch generates an interface structure that does not belong to either. In other words, they are incompatible. As reported in [34], this interface brings significant thermodynamical and kinetical barriers of nucleation. Although we have also proposed the nucleation concept for the silicon GB in 3.4, the mismatch simply coherently stretches adjacent units without generating an extra interface structure because the structural units involved in the phase transition are compatible. In this way, the difference between the nucleation barrier and growth barrier for a phase transition in the copper GB is much more significant than in the silicon GB. Therefore, the unit structures of the copper GB cannot perform transitions independently because of the inevitable generation of the interface structure. Instead, the phase transition is dominated by the migration of the interface. These features of 1) two well-defined non-identical phases, 2) a uniquely determined transition temperature, and 3) a transition process dominated by interface migration make the phase transition of the copper GB to be first-ordered. On the other hand, the silicon GB has structural units capable of transforming independently because all the structures inducing the phase transition are compatible. As discussed in 3.3, such flexibility brings various possibilities of the domain structures of which each has a distinctive free energy curve so that the phase transition does not have a well-defined

transition temperature, thus giving a second-ordered phase transition.

One might notice that each phase of the copper GB reported in [16] also has two degenerate states by orientational features because its structural unit is as well asymmetric as that of the Up or Down state of the silicon GB. The interesting question is whether it has a reconstruction behavior to shift between the two degenerate states. The answer should be negative because the degenerate states in copper are Incompatible.

From the discussion above, we can conclude that the intrinsic difference between the phase behaviors of the copper GB and the silicon GB is the compatibility of the two representative structures inducing the phase transition. Incompatible phase transition of the copper GB requires significant displacement of atoms at the boundary of the structural unit, inevitably making an interface structure that does not belong to either of the two representative states. The compatible phase transition of the silicon GB only significantly displaces atoms inside the unit cell, where the mismatch only generates lattice distortion without making an interface. Incompatible transition is dominated by the interface migration driven by the free energy difference between two well-defined pristine GB phases, thus having a uniquely determined transition temperature. Compatible phase transition is dominated by the competition of the entropy effects and the internal energy increase caused by the lattice distortion as a result of the interaction between opposite domains, where the various possibilities of domain structures with distinctive free energy curves make the phase transition to be second-ordered. Such a different extent of compatibility of silicon and copper GBs can be attributed to the difference in the properties of chemical bonds. When introducing a perturbation to a stabilized structure by displacing certain localized groups of atoms, a metallic-bonded system often results in a much larger range of significant structural variation than a covalent-bonded system. In other words, metallic-bonded systems are less likely to be tolerant of localized structural perturbations than covalent-bonded systems. This can be reflected by the fact that the silicon GBs have much more physically non-identical metastates than the metallic GBs [9].

Besides this well-known silicon GB, we have also found another

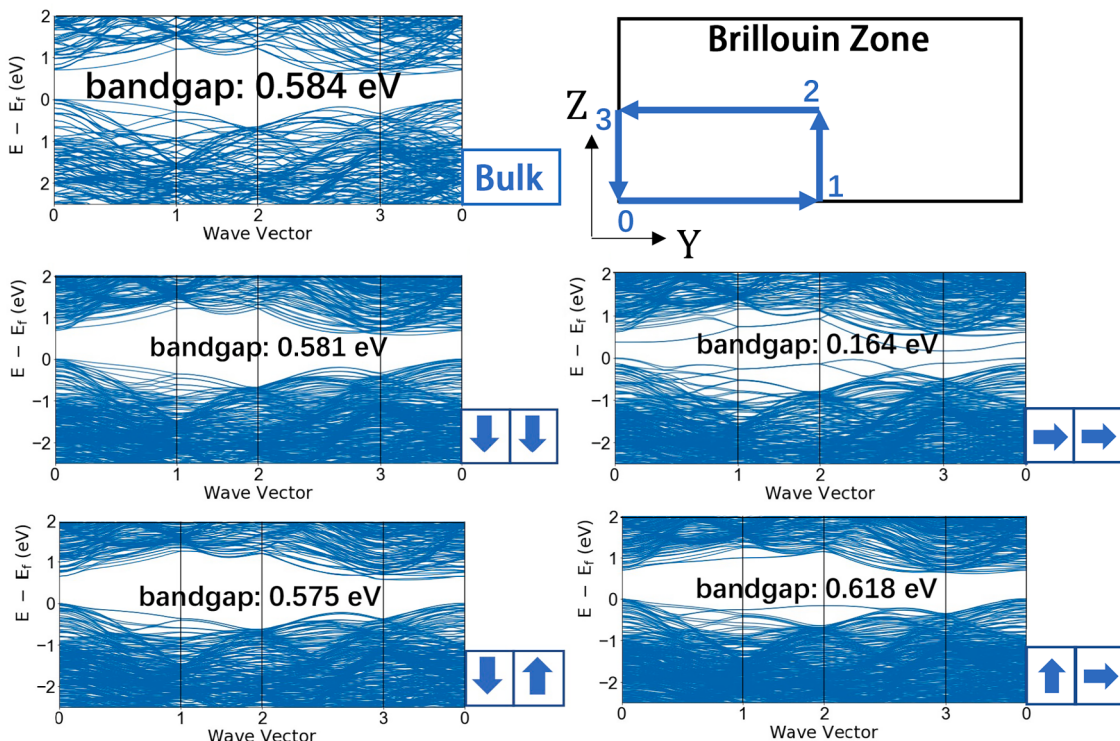


Fig. 7. Band structure of GBs comprising two units of different states.

symmetric tilt  $\langle 001 \rangle$  silicon GB having compatible reconstruction structures inducing a phase transition at about 750 K, which can be seen in Supplementary Materials S3. We believe that similar phase behaviors can also be found in other silicon GBs and GBs of different materials with covalent bonds.

### 3.6. Electronic structures

To understand the impact of the structural reconstruction on the device properties, following the method by Kohyama & Yamamoto [28], where a k-path in the two-dimensional Brillouin zone lying in the GB plane was applied, we calculated the band structure of four GBs comprising two structural units as shown in Fig. 7. Due to the limitation of the DFT-GGA method, the band gap of bulk silicon was simulated to be lower than the experimental value. However, considering the consistency in systematic error, this is not a significant problem for our investigation of the effects of reconstruction on the band structures. The computed band structures show that introducing bridge-state units generates extra bands into the band gap while mixing Up and Down states does not significantly affect the band structure. We also found that these extra bands generated by the bridge-state units are localized at the GB region, as shown in Supplementary Material S2, which can act as recombination centers in semiconductors. Although the defects by disorientation and the existence of bridge states are not likely to be significantly activated at a device-functioning temperature according to the HTST results, they can be kinetically trapped at low temperatures. For instance, according to HTST computation, a bridge state in a pure ground GB has an average lifetime of about only 1 s at 300 K but more than 36 days at 200 K before it jumps to the ground state. These results motivate exploring other GBs with similar reconstruction behaviors, which can generate manipulatable device performances with more significant modification to the band structure and higher equilibrium constant.

## 4. Conclusion

We presented a non-reported reconstruction mechanism of a well-known silicon GB between two degenerate ground states. The reconstruction path passes through one of two degenerate bridge states. We have verified the stability of the ground and bridge states at 0 K using DFT simulation for silicon, germanium, and diamond (carbon). The conclusion made for silicon GBs will likely be adapted to germanium and diamond (carbon) GBs. Previous studies have suggested that the covalent-bonded GBs possess much more metastates than the metallic-bonded GBs. These metastates were thought to affect the structural variation at elevated temperatures. Our thermodynamical and kinetical studies show that this well-known GB's structural variation at high temperatures is more likely to be dominated by the reconstruction states proposed in this work than by other previously reported metastates. The reconstruction mechanism also allows this well-known GB to be treated as a tessellation of the one-dimensional chains of the Ising model, where the interactions between Up and Down units are only significant in one dimension. Using HTST, we computed the reconstruction's transition rates and equilibrium constants for a single unit under different neighboring environments at elevated temperatures. We proposed an explanation for the reason causing disparity in phase transitions of this silicon GB and of a previously reported copper GB, which are both non-diffusive. That is the difference in the compatibility of the two representative structures inducing phase transition, which derives from the intrinsic disparity between the metallic and covalent bonds. Finally, we have shown that the reconstruction can affect the functional properties of the GB by modifying the band structure, which brings motivation to explore phase transitions of other GBs in crystalline semiconductors as they can generate novel manipulatable device performances. The methods applied in this work can also be used for other GBs and interfaces of materials with covalent bonds, which comprise reconstruction units.

## Declaration of Competing Interest

The authors declare that they have no known competing financial interests or personal relationships that could have appeared to influence the work reported in this paper.

## Acknowledgments

Yaoshu Xie is supported by Ministry of Education, Culture, Sports, Science and Technology (MEXT) Scholarship with Embassy Recommendation for Chinese students. This study is supported by JST-CREST (JPMJCR1993); MEXT (Nos 19H00818, and 19H05787); and Tenkai special funding in Institute of Industrial Science.

## Supplementary materials

Supplementary material associated with this article can be found, in the online version, at doi:10.1016/j.actamat.2023.118827.

## References

- [1] T. Watanabe, Grain boundary engineering: historical perspective and future prospects, *J. Mater. Sci.* 46 (2011) 4095–4115, <https://doi.org/10.1007/s10853-011-5393-z>.
- [2] A.R. Krause, P.R. Cantwell, C.J. Marvel, C. Compson, J.M. Rickman, M.P. Harmer, Review of grain boundary complexion engineering: know your boundaries, *J. Am. Ceram. Soc.* 102 (2019) 778–800, <https://doi.org/10.1111/jace.16045>.
- [3] R. Raghunathan, E. Johlin, J.C. Grossman, Grain boundary engineering for improved thin silicon photovoltaics, *Nano Lett.* 14 (2014) 4943–4950, <https://doi.org/10.1021/nl501020q>.
- [4] M. Mohr, L. Daccache, S. Horvat, K. Brühne, T. Jacob, H.J. Fecht, Influence of grain boundaries on elasticity and thermal conductivity of nanocrystalline diamond films, *Acta Mater.* 122 (2017) 92–98, <https://doi.org/10.1016/j.actamat.2016.09.042>.
- [5] W. Takeuchi, N. Taoka, M. Kurosawa, M. Sakashita, O. Nakatsuka, S. Zaima, High hole mobility tin-doped polycrystalline germanium layers formed on insulating substrates by low-temperature solid-phase crystallization, *Appl. Phys. Lett.* 107 (2015), 022103, <https://doi.org/10.1063/1.4926507>.
- [6] S. von Alftan, P.D. Haynes, K. Kaski, A.P. Sutton, Are the structures of twist grain boundaries in silicon ordered at 0 K? *Phys. Rev. Lett.* 96 (2006), 055505 <https://doi.org/10.1103/PhysRevLett.96.055505>.
- [7] M. Kohyama, R. Yamamoto, M. Doyama, Structures and energies of symmetrical  $\langle 011 \rangle$  tilt grain boundaries in silicon, *Phys. Stat. Sol. B* 137 (1986) 11–20, <https://doi.org/10.1002/pssb.2221370102>.
- [8] L. Wang, W. Yu, S. Shen, Revisiting the structures and energies of silicon  $\langle 110 \rangle$  symmetric tilt grain boundaries, *J. Mater. Res.* 34 (2019) 1021–1033, <https://doi.org/10.1557/jmr.2018.437>.
- [9] J. Han, V. Vitek, D.J. Srolovitz, Grain-boundary metastability and its statistical properties, *Acta Mater.* 104 (2016) 259–273, <https://doi.org/10.1016/j.actamat.2015.11.035>.
- [10] H. Hojo, T. Mizoguchi, H. Ohta, S.D. Findlay, N. Shibata, T. Yamamoto, Y. Ikuhara, Atomic structure of a  $\text{CeO}_2$  grain boundary: the role of oxygen vacancies, *Nano Lett.* 10 (2010) 4668–4672, <https://doi.org/10.1021/nl1029336>.
- [11] J.L. Piedeman, G.B. Thompson, The influence of alloying in stabilizing a faceted grain boundary structure, *Acta Mater.* 201 (2020) 329–340, <https://doi.org/10.1016/j.actamat.2020.09.085>.
- [12] P.R. Cantwell, M. Tang, S.J. Dillon, J. Luo, G.S. Rohrer, M.P. Harmer, Grain boundary complexions, *Acta Mater.* 62 (2014) 1–48, <https://doi.org/10.1016/j.actamat.2013.07.037>.
- [13] T. Frolov, D.L. Olmsted, M. Asta, Y. Mishin, Structural phase transformations in metallic grain boundaries, *Nat. Commun.* 4 (2013) 1–7, <https://doi.org/10.1038/ncomms2919>.
- [14] T. Frolov, W. Setyawan, R.J. Kurtz, J. Marian, A.R. Oganov, R.E. Rudd, Q. Zhu, Grain boundary phases in bcc metals, *Nanoscale* 10 (2018) 8253–8268, <https://doi.org/10.1039/c8nr00271a>.
- [15] Q. Zhu, A. Samanta, B. Li, R.E. Rudd, T. Frolov, Predicting phase behavior of grain boundaries with evolutionary search and machine learning, *Nat. Commun.* 9 (2018) 467, <https://doi.org/10.1038/s41467-018-02937-2>.
- [16] T. Meiners, T. Frolov, R.E. Rudd, G. Dehm, C.H. Liebscher, Observations of grain-boundary phase transformations in an elemental metal, *Nature* 579 (2020) 375–378, <https://doi.org/10.1038/s41586-020-2082-6>.
- [17] M.A. Tschopp, D.L. McDowell, Asymmetric tilt grain boundary structure and energy in copper and aluminium, *Philos. Mag.* 87 (2007) 3871–3892, <https://doi.org/10.1080/14786430701455321>.
- [18] S. Plimpton, Fast parallel algorithms for short-range molecular dynamics, *J. Comput. Phys.* 117 (1995) 1–19, <https://doi.org/10.1006/jcph.1995.1039>.
- [19] G.P.P. Pun, Y. Mishin, Optimized interatomic potential for silicon and its application to thermal stability of silicene, *Phys. Rev. B* 95 (2017), 224103, <https://doi.org/10.1103/PhysRevB.95.224103>.

- [20] J. Tersoff, Modeling solid-state chemistry: interatomic potentials for multicomponent systems, Phys. Rev. B 39 (1989) 5566–5568, <https://doi.org/10.1103/PhysRevB.39.5566>.
- [21] J. Nord, K. Albe, P. Erhart, K. Nordlund, Modelling of compound semiconductors: analytical bond-order potential for gallium, nitrogen and gallium nitride, J. Phys. Condens. Matter 15 (2003) 5649–5662, <https://doi.org/10.1088/0953-8984/15/32/324>.
- [22] A. Stukowski, Visualization and analysis of atomistic simulation data with OVITO—the open visualization tool, Model. Simul. Mater. Sci. Eng. 18 (2009) 15012, <https://doi.org/10.1088/0965-0393/18/1/015012>.
- [23] G. Kresse, J. Furthmüller, Efficient iterative schemes for *ab initio* total-energy calculations using a plane-wave basis set, Phys. Rev. B 54 (1996) 11169, <https://doi.org/10.1103/PhysRevB.54.11169>.
- [24] G. Kresse, D. Joubert, From ultrasoft pseudopotentials to the projector augmented-wave method, Phys. Rev. B 59 (1999) 1758, <https://doi.org/10.1103/PhysRevB.59.1758>.
- [25] G. Henkelman, H. Jónsson, Improved tangent estimate in the nudged elastic band method for finding minimum energy paths and saddle points, J. Chem. Phys. 113 (2000) 9978, <https://doi.org/10.1063/1.1323224>.
- [26] G. Henkelman, B.P. Uberuaga, H. Jónsson, A climbing image nudged elastic band method for finding saddle points and minimum energy paths, J. Chem. Phys. 113 (2000) 9901, <https://doi.org/10.1063/1.1329672>.
- [27] E. Maras, O. Trushin, A. Stukowski, T. Ala-Nissila, H. Jónsson, Global transition path search for dislocation formation in Ge on Si(001), Comput. Phys. Commun. 205 (2016) 13–21, <https://doi.org/10.1016/j.cpc.2016.04.001>.
- [28] M. Kohyama, R. Yamamoto, Theoretical study of grain boundaries in Si: effects of structural disorder on the local electronic structure and the origin of band tails, Phys. Rev. B 50 (1994) 8502–8522, <https://doi.org/10.1103/PhysRevB.50.8502>.
- [29] M.T. Dove, Theory of displacive phase transitions in minerals, Am. Mineral. 82 (1997) 213–244, <https://doi.org/10.2138/AM-1997-3-401>.
- [30] K.E. Khor, S.Das Sarma, Proposed universal interatomic potential for elemental tetrahedrally bonded semiconductors, Phys. Rev. B 38 (1988) 3318–3322, <https://doi.org/10.1103/PhysRevB.38.3318>.
- [31] T. Kumagai, S. Izumi, S. Hara, S. Sakai, Development of bond-order potentials that can reproduce the elastic constants and melting point of silicon for classical molecular dynamics simulation, Comput. Mater. Sci. 39 (2007) 457–464, <https://doi.org/10.1016/j.commatsci.2006.07.013>.
- [32] F.H. Stillinger, T.A. Weber, Computer simulation of local order in condensed phases of silicon, Phys. Rev. B 31 (1985) 5262, <https://doi.org/10.1103/PhysRevB.31.5262>.
- [33] R. Freitas, R.E. Rudd, M. Asta, T. Frolov, Free energy of grain boundary phases: atomistic calculations for  $\Sigma 5(310)[001]$  grain boundary in Cu, Phys. Rev. Mater. 2 (2018), 093603, <https://doi.org/10.1103/PhysRevMaterials.2.093603>.
- [34] I.S. Winter, R.E. Rudd, T. Oppelstrup, T. Frolov, Nucleation of grain boundary phases, Phys. Rev. Lett. 128 (2022), 035701, <https://doi.org/10.1103/PhysRevLett.128.035701>.
- [35] K.J. Laidler, M.C. King, Development of transition-state theory, J. Phys. Chem. 87 (1983) 2657–2664, <https://doi.org/10.1021/j100238a002>.
- [36] G.H. Vineyard, Frequency factors and isotope effects in solid state rate processes, J. Phys. Chem. Solids 3 (1957) 121–127, [https://doi.org/10.1016/0022-3697\(57\)90059-8](https://doi.org/10.1016/0022-3697(57)90059-8).